IMPACTS OF INVERTER-BASED RESOURCES CONTROLS ON DISTANCE PROTECTION

Mamadou S Diallo, Raphaël Caire, Christophe Ghafari, Christian Guibout, Bertrand Raison

IMPACTS OF INVERTER-BASED RESOURCES CONTROLS ON DISTANCE PROTECTION

Mamadou S DIALLO[1], Raphaël CAIRE[1], Christophe GHAFARI [2], Christian GUIBOUT[3], Bertrand RAISON[1]

[1]*Univ. Grenoble Alpes, CNRS, Grenoble INP, G2Elab, 38000 Grenoble, France*
[2] *RTE, 69330 Jonage, France*
[3] *RTE, 92800 Puteaux, France*

Keywords: DISTANCE PROTECTION, INVERTER-BASED RESOURCES, POWER TRANSMISSION LINE

Abstract

The penetration of Inverter-Based Resources (IBRs) into the grid increased significantly in recent years. This poses a significant challenge to distance protection (DP). In fact, DP has been designed based on the behaviour of synchronous generator (SG) during faults. The behaviours of SGs and IBRs during faults are very different. Today, DP is used to protect transmission lines interconnected with IBRs. RTE, the French TSO, facing an increasing integration of IBRs is questioning its interconnection specifications in terms of selectivity support. This paper presents an analysis of the phase currents injected by a wind turbine using coupled sequence control (CSC) and decoupled sequence control (DSC) and their potential impact on the DP, in particular on phase selection. This study is carried out by using the EPRI benchmark FSC available in EMTP-RV. The results show that with CSC control, a single-phase-to-earth fault with low fault resistance, behaves as a phase-to-phase fault. Conversely, a phase-to-phase fault behaves as a single phase-to-earth fault. This can lead to incorrect selection of the faulted phase. The results also show that with DSC control, there is a slight improvement in the injection of negative sequence current compared to CSC control.

1. Introduction

The penetration of Inverter-Based Resources (IBRs) into the power system presents a significant challenge for the power system protections (PSPs), particularly distance protection (DP). PSPs have been designed based on the behaviour of synchronous generator (SG). The negative sequence current (I_2) contributed by the SG during unbalanced faults is significantly high compared to the negative sequence current injected by IBRs and the angle between the negative sequence voltage (V_2) and I_2 is typically around 90° [1], [2]. The behaviour of IBRs during faults is totally different from SG due to the current limitation by the control of IBRs. The former IBRs used the Coupled Sequence Control (CSC) scheme which does not allow to inject I_2 during unbalanced faults. However, there is a small I_2 value still exists due to the unbalanced voltage created into the network. Today, Decoupled Sequence Control (DSC) is required by almost all TSOs in order to inject the positive sequence current (I_1) and I_2 simultaneously during faults. However, the magnitude of the total current injected by IBRs is still limited to 1.2 p.u.

Many papers in the literature discuss about the impacts of IBRs on power system protection, such as [3], [4], [5]. However, there is a lack of research on the potential impact of Single Line to Earth (SLE) faults behaving as Line-Line to Earth faults (LLE) and Line-Line fault (LL) or LLE behaving as SLE faults on distance relays that use phase currents to perform the phase selection. This paper explains the behaviour of the phase currents injected by a Wind Turbine (WT) during SLE, LL and LLE faults using CSC and DCS controls.

2. Wind Turbine Model

This study is conducted by using the EPRI Benchmark FSC (Full Scale Converter) model available in EMTP-RV and this model includes the coupled sequence control (CSC) and decoupled sequence control (DSC). The vector group of the MV/HV transformer (Tr) of the wind turbine is dYn. The neutral is directly earthed. In general, the French TSO, RTE, sets an impedance for earthing the neutral of the HV transformers. To comply with this practice, a 38Ω reactance has been added to the Tr neutral of the WT model. The parameters of the WT model can be found in EMTP-RV model and those of the line are given in Table 1.

Table 1 Line parameters

Line parameters					
$X_1[\Omega]$	$X_0[\Omega]$	$R_1[\Omega]$	$R_0[\Omega]$	$C_1[\mu F]$	$C_0[\mu F]$
20	67	3	10	460	260

Where, X_1, R_1, C_1, X_0, R_0 and C_0 are the positive and zero sequences of reactance, resistance and capacitance respectively.

In the following sections 2.1 and 2.2, the CSC and DSC control schemes will be brief discussed.

2.1. Coupled Sequence Control Scheme

The positive sequence current which will be injected by the WT with the CSC control during faults is defined as:

$$\underline{I_1} = I_d + jI_q \quad (1)$$

With:

- $I_q = k\Delta V_1$ and $2 \le k \le 6$
- $I_d = \sqrt{I_{maxi}^2 - I_q^2}$
- $I_{maxi} \le 1.2$ p. u.

I_d and I_q are d-q axis current in per-unit. I_{maxi} is the maximum current of the inverter and V_1 is the positive sequence voltage in p.u. Usually the positive sequence of the voltage dip is calculated using (2), but this WT model uses (3):

$$\Delta V_1 = 1 - V_1 \quad (2)$$

$$\Delta V_1 = V_{mem} - V_1 \quad (3)$$

V_{mem} is the memorized voltage. It is memorized for 250ms.

$\underline{I}_1$ can be written as (1) [6]:

$$\underline{I}_1 = I_1 e^{j\left[\tan^{-1}\left(\frac{I_q}{I_d} + (\angle \underline{V}_1)\right)\right]} \quad (4)$$

As it can be seen from (4), the angle of $\underline{I}_1$ depends both d and q currents axis injected and the angle of $\underline{V}_1$.

For more information on the CSC control scheme of the Grid Following (GFL) inverter, please refer to [7], [8].

2.2. *Decoupled Sequence Control Scheme*

The positive and negative phasor currents, $\underline{I}_1$ and $\underline{I}_2$ which will be injected by the inverter during faults can be written as [6]:

$$\underline{I}_1 = I_1 e^{j\left[\tan^{-1}\left(\frac{I_q}{I_d} + (\angle \underline{V}_1)\right)\right]} \quad (5)$$

$$\underline{I}_2 = I_2 e^{j\left[\tan^{-1}(90 + (\angle \underline{V}_2))\right]} \quad (6)$$

Where, $\underline{V}_2$ is the negative sequence voltage. According to (6), the angle of $\underline{I}_2$ depends on the negative-sequence voltage. For more information on DSC control scheme, please refer to [9].

3. Analysis of Fault Phase Currents of Wind Turbine Using the CSC Control Scheme

This section analyses the phase currents injected by the WT during Single Line-to-Earth (SLE), line-to-line (LL), and Line-to-Line-to-Earth faults will be analysed.

To analyse the phase currents of the WT during faults, a methodology is used to construct and analyse the real and imaginary parts of the phase currents, as shown in Fig. 1. The simulation results of different faults into EMTP-RV are exported to COMTRADE files [10]. Then, the COMTRADE files are imported in MATLAB/Simulink. The zero, positive and negative sequence phasor currents are then calculated. The real and imaginary parts of the phase A, B and C currents obtained from the zero, positive and negative sequence currents are used in the following analysis.

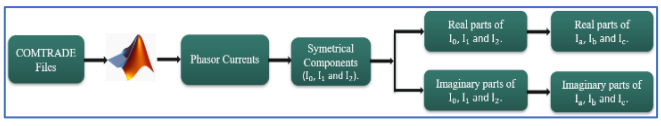

Fig. 1 Methodology

To explain the behaviour of the phase currents injected by the WT during SLE, LL and LLE faults, the phasor currents are used to analyse the impact of the phase angle between the positive, negative and the zero sequence currents on the phase currents.

The phasor currents can be written as (7):

$$\begin{cases} \underline{I}_a = \underline{I}_1 + \underline{I}_2 + \underline{I}_0 \\ \underline{I}_b = a^2\underline{I}_1 + a\underline{I}_2 + \underline{I}_0 \\ \underline{I}_c = a\underline{I}_1 + a^2\underline{I}_2 + \underline{I}_0 \end{cases} \quad (7)$$

Where, $\underline{I}_a$, $\underline{I}_b$, and $\underline{I}_c$ are the phasor currents of phases A, B, and C respectively. $\underline{I}_1$, $\underline{I}_2$, and $\underline{I}_2$ are the phasors of the positive, negative and zero sequence currents respectively. The phasor rotation operator a is equal to $-\frac{1}{2} + \frac{j\sqrt{3}}{2}$. Substituting a in (7) and also the real and imaginary parts of $\underline{I}_1$, $\underline{I}_2$ and $\underline{I}_2$ in (7), (8) is obtained:

$$\begin{cases} I_{ar} = I_{1r} + I_{2r} + I_{0r} \\ I_{br} = -\frac{1}{2}(I_{1r} + I_{2r}) + \frac{\sqrt{3}}{2}(I_{1i} - I_{2i}) + I_{0r} \\ I_{cr} = -\frac{1}{2}(I_{1r} + I_{2r}) + \frac{\sqrt{3}}{2}(-I_{1i} + I_{2i}) + I_{0r} \\ I_{ai} = I_{1i} + I_{2i} + I_{0i} \\ I_{bi} = -\frac{1}{2}(I_{1i} + I_{2i}) - \frac{\sqrt{3}}{2}(-I_{1r} + I_{2r}) + I_{0i} \\ I_{ci} = -\frac{1}{2}(I_{1i} + I_{2i}) + \frac{\sqrt{3}}{2}(I_{1r} - I_{2r}) + I_{0i} \end{cases} \quad (8)$$

I_{ar}, I_{br}, I_{cr} are the real parts of $\underline{I}_a$, $\underline{I}_b$ and $\underline{I}_c$. I_{ai}, I_{bi}, I_{ci} are the imaginary parts of $\underline{I}_a$, $\underline{I}_b$ and $\underline{I}_c$.

3.1. *Single Line to Earth Fault with Low Value of Fault Resistance*

To analyse the phase currents of the WT during SLE faults, a phase A to Earth (AE) fault with a fault resistance, R_F equal to 0.01Ω is simulated at 2 s for a 100 ms period. Fig. 2 shows the currents injected by the WT during the fault. The RMS phase currents values I_a, I_b, and I_c in the secondary side of current transformer (SSCT) are 1.48A, 1.55A and 0.42A respectively. As it can be seen in Fig. 2, AE fault currents are similar to those of a line-to-line fault. Furthermore, the current in phase B exceeds that of the faulted phase A.

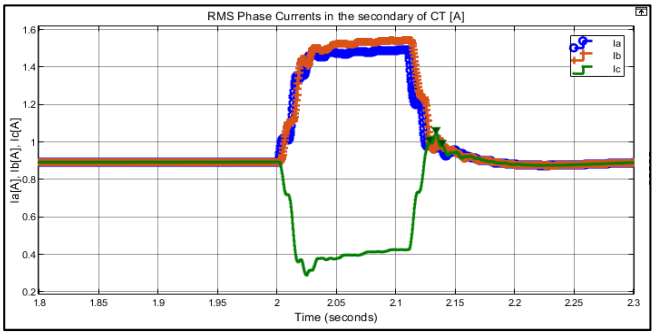

Fig. 2 RMS Phase Currents with CSC control

Despite the fact that the CSC control scheme does not allow to inject I_2, there is a small I_2 value due to the unbalance created into the grid during unbalance faults. However, for this study, first I_2 will be neglected.

3.1.1 The negative-sequence current is neglected: By neglecting I_2, (9) is obtained:

$$\begin{cases} I_{ar} = I_{1r} + I_{0r} \\ I_{br} = -\frac{1}{2}I_{1r} + \frac{\sqrt{3}}{2}I_{1i} + I_{0r} = Term1 + I_{0r} \\ I_{cr} = -\frac{1}{2}I_{1r} - \frac{\sqrt{3}}{2}I_{1i} + I_{0r} = Term2 + I_{0r} \\ I_{ai} = I_{1i} + I_{0i} \\ I_{bi} = -\frac{1}{2}I_{1i} - \frac{\sqrt{3}}{2}I_{1r} + I_{0i} = Term3 + I_{0r} \\ I_{ci} = -\frac{1}{2}I_{1i} + \frac{\sqrt{3}}{2}I_{1r} + I_{0i} = Term4 + I_{0r} \end{cases} \quad (9)$$

The equation system (9) is used to analyse the effects of the angles between I_{1r} and I_{0r}, Term1 and I_{0r}, Term2 and I_{0r} on I_{ar}, I_{br} and I_{cr} respectively.

The result of the AE fault with R_F equal to 0Ω is used to analyse I_{ar}. Fig. 3 shows the result of real part of $\underline{Ia}$ with its different terms. The maximum values of I_{1r} and I_{0r} in SSCT are 1.05A and 0.707A respectively. The angle between I_{1r} and I_{0r} is 75°. The maximum value of the real part of $\underline{Ia}$ is 1.409A. Since the angle between I_{1r} and I_{0r} is close to 90°, therefore, the result of I_{ar} which is the sum of I_{1r} and I_{0r} is not very high compare to I_{br}.

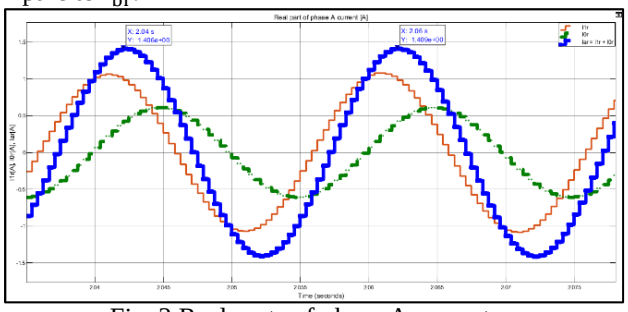

Fig. 3 Real parts of phase A current

To explain the impact of the angle between Term1 and the real part of zero sequence current on the real part of the phase B, the AE fault with $R_F = 0\Omega$ is used. Fig. 4 shows that the maximum values of Term1, I_{0r} and the angle between Term1 and I_{0r} are 1.093A, 0.611A and 45° respectively. The maximum value of I_{br} is 1.546A. Since the angle between Term1 and the I_{0r} is relatively small, much less than 90°, the real part of the $\underline{I_b}$ is high and greater than the real part of $\underline{I_a}$.

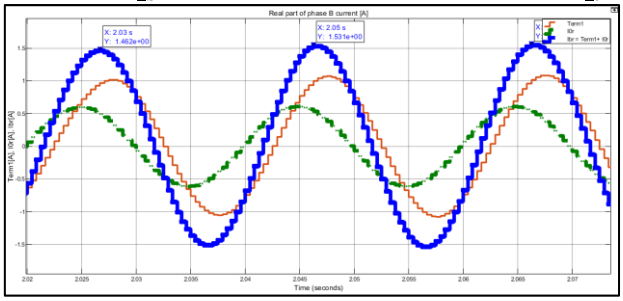

Fig. 4 Real parts of phase B current

To explain the impact of the angle between Term2 and the real part of the zero-sequence current on the real part of phase C, the AE fault with R_F equals to 0Ω is used. Fig. 5 shows that the maximum values of Term2, I_{0r} and the angle between Term2 and I_{0r} are 1.094A, 0.611A and 165° respectively. The maximum value of I_{cr} is 0.499A. As it can be seen in Fig. 5, the angle between Term2 and I_{0r} is very high, almost in phase opposition. Therefore, the real part of $\underline{I_c}$ is very low.

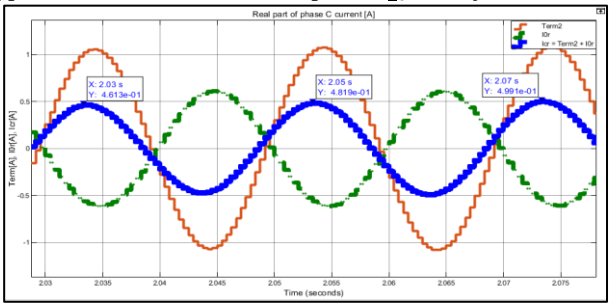

Fig. 5 Real parts of phase C current

Table 2 summarises the analysis performed on the imaginary parts of the three phase currents injected by the WT during the AE fault with R_F equals to 0Ω. Similar results are obtained for both the real and imaginary parts. The results observed in this section 3.1 show that, the smaller the angle between the positive and zero sequence currents, the higher the current value.

Table 2 Imaginary parts currents results

Imaginary Parts			
Max value of current [A]		Angle (φ) in [°]	
$\mathbf{I_{ai}}$	1.418	$\varphi(I_{1i}, I_{0i})$	75.24°
$\mathbf{I_{bi}}$	1.563	$\varphi(Term3, I_{0i})$	45.04°
$\mathbf{I_{ci}}$	0.517	$\varphi(Term4, I_{0i})$	165.24°

The effect of the negative sequence current on the phase currents of the WT during SLE fault with the CSC control will be discussed in the section 3.1.2.

3.1.2. The negative sequence current is considered: The same process carried out from (7) to (9) is carried out in this section. Considering $\underline{I_2}$, (10) is obtained:

$$\begin{cases} I_{ar} = I_{1r} + I_{2r} + I_{0r} = Term5 + I_{0r} \\ I_{br} = -\frac{1}{2}(I_{1r} + I_{2r}) + \frac{\sqrt{3}}{2}(I_{1i} - I_{2i}) + I_{0r} = Term6 + I_{0r} \\ I_{cr} = -\frac{1}{2}(I_{1r} + I_{2r}) + \frac{\sqrt{3}}{2}(-I_{1i} + I_{2i}) + I_{0r} = Term7 + I_{0r} \\ I_{ai} = I_{1i} + I_{2i} + I_{0i} = Term8 + I_{0r} \\ I_{bi} = -\frac{1}{2}(I_{1i} + I_{2i}) - \frac{\sqrt{3}}{2}(-I_{1r} + I_{2r}) + I_{0i} = Term9 + I_{0r} \\ I_{ci} = -\frac{1}{2}(I_{1i} + I_{2i}) + \frac{\sqrt{3}}{2}(I_{1r} - I_{2r}) + I_{0i} = Term10 + I_{0r} \end{cases} \quad (10)$$

The impacts of the angle between Term5 and I_{0r} on I_{ar} value, the angle between the Term6 and I_{0r} on I_{br} value and the angle between the Term7 and I_{0r} on I_{cr} value will be discussed respectively in this section. Table 3 shows the results of the real part values of the phase currents and the angles between their terms.

Table 3 Real parts currents results with the reverse current

Real Parts			
Max value of current [A]		Angle (φ) in [°]	
$\mathbf{I_{ar}}$	1.484	$\varphi(Term5, I_{0r})$	75,06°
$\mathbf{I_{br}}$	1.538	$\varphi(Term6, I_{0r})$	53.1°
$\mathbf{I_{cr}}$	0.589	$\varphi(Term7, I_{0r})$	165.02°

Table 4 shows the results of imaginary parts values of the phase currents and the angles between their terms.

Table 4 Imaginary parts currents results with I_2

Imaginary Parts			
Max value of current [A]		Angle (φ) in [°]	
$\mathbf{I_{ai}}$	1.488	$\varphi(\text{Term8}, I_{0i})$	75.00°
$\mathbf{I_{bi}}$	1.540	$\varphi(\text{Term9}, I_{0i})$	52.49°
$\mathbf{I_{ci}}$	0.424	$\varphi(\text{Term10}, I_{0i})$	165.17°

A comparison of the results obtained in sections 3.1.1 and 3.1.2 reveals that there is negligible variation between them. This indicates that the impact of I_2 on the phase current values can be neglected in case of SLE faults with a low value of R_F. However, it can be observed that the presence of I_2 slightly reduces the value of I_b and at the same time increases the value of I_a. This phenomenon will be more obvious when using DSC control.

The behaviour of phase currents of WT in case of a SLE fault with high values of R_F is discussed in the section 3.2.

3.2. Single Line to Earth Fault with high Value of Fault Resistance

In the case of a SLE fault with R_F, the equivalent circuit of the sequence network is shown in [11] and the superposition method is used to calculate the zero sequence current from the WT side. The expression of I_0 is given in (11).

$$I_0 = F_0 * \frac{E_{1R}}{(1-x)Z_{1L}+Z_{1R}+Z_{0eq}+Z_{2eq}+\mathbf{3R_F}} * F_1 \quad (11)$$

With :

- $F_0 = \frac{(1-x)Z_{0L}+Z_{0R}}{3Z_n+Z_{0Tr}+Z_{0L}+Z_{0R}}$
- $F_1 = 1 + \left((1-x)Z_{1L} + Z_{1R}\right) * \frac{I_1}{E_{1R}}$

Where, Z_{1Tr}, Z_{1L}, Z_{1R}, Z_{2Tr}, Z_{2L}, Z_{2R}, Z_{0Tr}, Z_{0L}, Z_{0R} are the positive, negative and zero sequence impedances of MV/HV transformer, line and the grid respectively. Z_n, is the neutral impedance of transformer. Z_{0eq} and Z_{2eq} are the zero and negative sequence equivalent impedances respectively. Z_{0eq} and Z_{2eq} are calculated using the Thevenin method. E_{1R}, I_1 and x are the voltage source of grid, positive sequence current of the WT and the fault distance respectively.

As it can be seen in (11), the higher the R_F value, the smaller the I_0 value. Table 5 shows the phase currents results of SLE faults for different R_F values. As it can be seen, I_0 decreases when R_F increases and, at the same time, phase A current value is greater than the phase B current value. This means that R_F reduces the impact of I_0 on the phase currents.

Table 5 Phase current variation according the fault resistance

RMS values of phase currents				
$\mathbf{R_F}$ [Ω]	0.01	10	30	50
$\mathbf{I_0}$ [A]	0.626	0.609	0.518	0.428
$\mathbf{I_a}$ [A]	1.492	1.537	1.505	1.220
$\mathbf{I_b}$ [A]	1.543	1.488	1.323	1.017
$\mathbf{I_c}$ [A]	0.424	0.396	0.406	0.699

3.3. Line to Line fault

To analyse the behaviour of WT phase currents during LL faults, an AB fault with fault resistance, R_F equal to 0Ω is simulated at 2 s for a period of 100 ms. Fig. 6 shows the currents injected by the WT during the fault. The RMS current values of I_a, I_b and I_c in the SSCT are 1.06A, 1.44A and 1.11A respectively. As it can be seen in this figure, these currents resemble those of a phase B to earth fault. This indicates that a relay using phase currents for phase selection may incorrectly identify the faulty phase as B in this case and subsequently trip only one phase, when all three phases should be tripped.

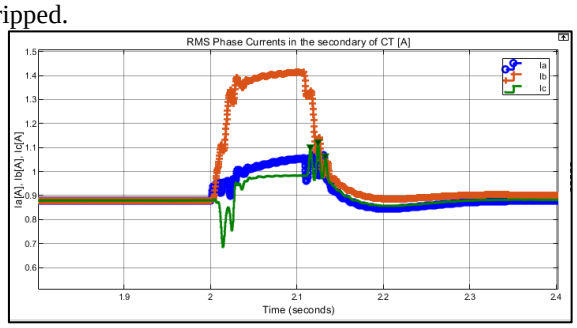

Fig. 6 AB fault result with CSC control

The behaviour of phase currents of WT during AB fault is analysed below. Since there is no I_0 in the case of LL fault, $I_0 = 0$ and first, I_2 is not considered, so (12) is obtained.

$$\begin{cases} \underline{I}_a = I_{1r} + jI_{1i} \\ \underline{I}_b = -\frac{1}{2}I_{1r} + \frac{\sqrt{3}}{2}I_{1i} + j\left(-\frac{1}{2}I_{1i} - \frac{\sqrt{3}}{2}I_{1r}\right) \\ \underline{I}_c = -\frac{1}{2}I_{1r} - \frac{\sqrt{3}}{2}I_{1i} + j\left(-\frac{1}{2}I_{1i} + \frac{\sqrt{3}}{2}I_{1r}\right) \end{cases} \quad (12)$$

Fig. 7 shows the result of (12). As the three phase currents contain only I_1, their values are equal.

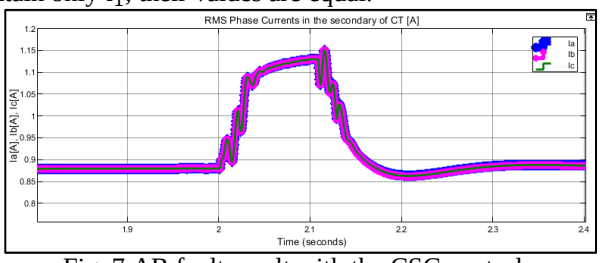

Fig. 7 AB fault result with the CSC control

Secondly, I_2 is considered and is added to (12). The result is shown in Fig. 6. By comparing Fig. 6 and Fig. 7, it can be observed that the increase in the phase B current value compared to phases A and C is due to the presence of I_2 on the WT side. Although the value of I_2 with the CSC is very low, however, it still impacts the phase currents in case of LL faults because the I_1 value of the WT is small, less than 1.2 p.u. This could potentially lead to a single-phase trip, when all three phases should be tripped.

The behaviour of phase currents of WT during ABE fault is discussed in section 3.4.

3.4. Line to Line to Earth Fault

To analyse the behaviour of WT phase currents, an ABE fault with R_F equal to 0Ω is simulated at 2 s for a 100 ms period. The RMS values of I_a, I_b and I_c in the SSCT are 1.968A, 0.824A and 0.679A respectively. As it can be seen in Fig. 8, the current waveforms obtained during the ABE fault are similar to the theorical waveforms of a BE fault, as the same case for AB fault in the section 3.3. The only difference

between the scenarios in 3.3. and 3.4 is the magnitude of the phase currents due to the presence of I_0 during the fault. In this case also, this could potentially lead to a single-phase, when all three phases should be tripped.

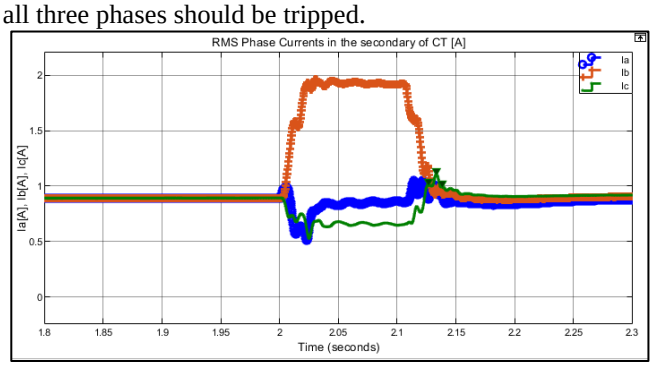

Fig. 8: ABE fault result with the CSC control

4. Analysis of the Phase Currents during faults with the DSC Control Scheme

Section 4 determines whether the phase currents injected by the WT with DSC control scheme differ from those with CSC control and assesses how DSC control improves phase selection.

An SLE fault is first analysed in section 4.1. Then, the impact of R_F on I_0 during SLE faults and how it changes the phase currents is discussed in the section 4.2. The LL and LLE faults are discussed in sections 4.3. and 4.4 respectively.

4.1. Single Line to Earth Fault

An AE fault with R_F equal 0.01Ω is simulated at 2 s for a period of 100 ms. Fig. 9 shows the currents of WT with DSC control. The RMS current values of phases A, B and C in SSCT are 1.66A, 1.38A and 0.437A. The initial observation derived from this result is that the values of the phases A and B currents increased during the occurrence of the fault. This can lead to an incorrect phase selection and conduct to a three-phase tripping, when it is only one phase should be tripped. The second observation is that the current value of phase A is greater than the current of phase B. This behaviour is different from the same fault (AE) with CSC control. Since I_2 value of the WT with the DSC control is slightly high, this reduced the impact of I_0 on the phase currents. Therefore, the current value of the phase B is reduced and the current of the phase A is increased. However, the I_2 value is not sufficient to ensure that only the phase A increased during the AE fault, as is the case with the SG behaviour during SLE faults.

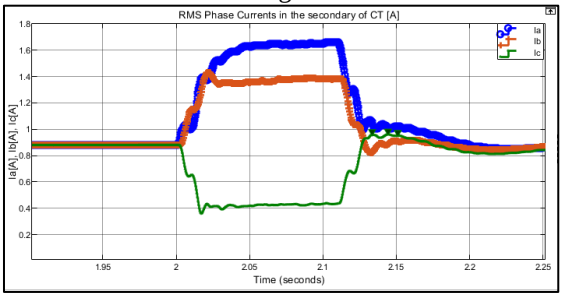

Fig. 9: AE fault result with DSC control

4.2. Single Line to Earth Fault with different values of Fault Resistance

Table 6 shows the results of phase currents and I_0 in the case of an AE faults for different R_F values. As it can be seen, the more the R_F values, the less the I_0 values and at the same time, the currents values of the faulted phase A are bigger than the current values of the phase B. It means that, in case of SLE fault with high value of R_F, the profile of the WT phase currents is similar that of SG. However, the current magnitudes of SG are much higher than those of IBRs.

Table 6: RMS values of phase currents with the DSC control

$\mathbf{R_F}$ [Ω]	0.01	10	30	50
$\mathbf{I_0}$ [A]	0.755	0.682	0.464	0.330
$\mathbf{I_a}$ [A]	1.660	1.658	1.423	1.317
$\mathbf{I_b}$ [A]	1.383	1.199	1.056	0.973
$\mathbf{I_c}$ [A]	0.437	0.205	0.381	0.603

4.3. Line to Line fault

An AB fault with R_F equal to 0Ω is simulated at 2 s for a duration of 100 ms. Fig. 10 shows the currents of the WT with DSC control. The current values of phases A, B and C are 0.846A, 1.342A and 0.603A respectively. These current waveforms are similar to those of a theorical BE fault. By comparing the results shown in Fig. 6 and Fig. 10, it can be observed that the results are very similar. The small difference between them is that, in the case of an AB fault with the DSC control, the impact of I_2 on the phase currents is more significant than in the case of an AB fault with CSC control. The current of phase A increases at the beginning of the fault and then decreases. This is due to the fact that 1.5 cycles are necessary for I_2 to reach its steady state value. As the value of I_1 increases during the fault and the value of I_2 is very low at the beginning, the sum of them increases. When I_2 reaches its steady state value, the angle between I_1 and I_2 is 113.09°. As this angle is greater than 90°, the sum of I_1 and I_2 decreases. This is why the current value of phase A decreases after 1.5 cycles.

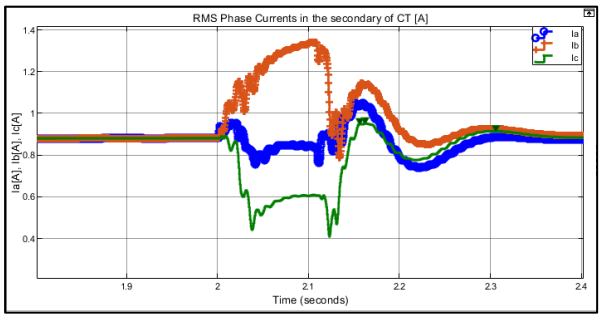

Fig. 10: AB fault result with DSC

4.4. Line to Line to Earth fault

Fig. 11 shows the result of an ABE fault with R_F equal to 0Ω which is simulated at 2 s for a 100 ms period. The values of phases A, B and C are 1.715A, 1.286A and 0.256A respectively. As it can be seen in Fig. 11, the currents of the WT with DSC control during ABE fault demonstrate a high degree of similarity to those injected with CSC control during

AB fault. The small different between them is that the current of the phase A decreases at the beginning of the fault and then increases. This can be explained by the fact that I_2 is almost equal to zero for more than two cycles. At that time, the angle between of ($I_1 + I_2$) and I_0 is around 142.3° which is much greater than 90°. Therefore, the value of I_a decreases at the beginning of the fault.

When I_2 reaches its steady state value, the angle between $(I_1 + I_2)$ and I_0 is about 90°. Therefore, the sum of I_1, I_2 and I_0 (which is equal to I_a), increases slightly. The presence of I_0 during the ABE fault yields higher values of I_a and I_b compared to the AB fault seen before.

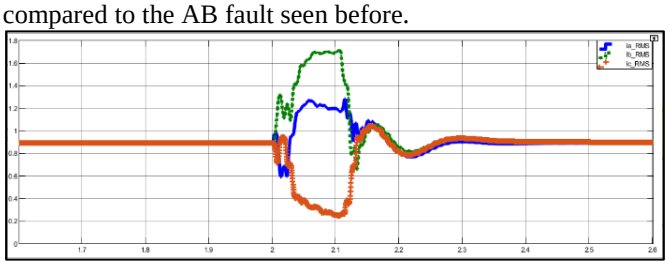

Fig. 11: ABE fault result with DSC control

5. Conclusion

The purpose of this paper is to analyse the behaviour of the phase currents injected by a wind turbine during SLE, LL and LLE faults with the CSC and DCS controls. The potential impact on the phase selection of the distance protection is also analysed in the paper. The EPRI Benchmark FSC version 4 model available in EMTP-RV including the CSC and DSC controls is used for this study. The study's findings indicate that the behaviour of the phase current injected by the WT during a SLE fault with a low fault resistance value is analogous to that of LL or LLE faults, attributable to the impact of zero-sequence current on the phase currents. Conversely, the phase currents injected by the WT with CSC and DSC control during an LL faults with a low value of the fault resistance are similar to an SLE fault due to the negative sequence current present during LL faults. Even though the CSC control does not allow the injection of negative sequence current, there is a small value of negative sequence current which impacts the phase currents. The phase currents are more impacted by the negative sequence current during a LL with the DSC control than with the CSC control, because the value of the negative sequence current is higher with the DCS control than with the CSC control. The results also show that the phase currents are more impacted during LLE faults than LL faults due to the presence of zero-sequence current during the faults.

5 Acknowledgements

This work is funded by the French TSO RTE.

6 References

[1] 'Impact of Inverter-Based Resources on Protection Schemes Based on Negative Sequence Components'. Accessed: Dec. 16, 2024. [Online]. Available: https://www.epri.com/research/products/000000003002016197

[2] G. Kou, J. Jordan, B. Cockerham, R. Patterson, and P. VanSant, 'Negative-Sequence Current Injection of Transmission Solar Farms', *IEEE Transactions on Power Delivery*, vol. 35, no. 6, pp. 2740–2743, Dec. 2020, doi: 10.1109/TPWRD.2020.3014783.

[3] A. Haddadi, E. Farantatos, I. Kocar, and U. Karaagac, 'Impact of Inverter Based Resources on System Protection', *Energies*, vol. 14, no. 4, p. 1050, Feb. 2021, doi: 10.3390/en14041050.

[4] E. Martínez Carrasco, M. P. Comech Moreno, M. T. Villén Martínez, and S. Borroy Vicente, 'Improved Faulted Phase Selection Algorithm for Distance Protection under High Penetration of Renewable Energies', *Energies*, vol. 13, no. 3, p. 558, Jan. 2020, doi: 10.3390/en13030558.

[5] Y. Feng, Z. Zhang, Q. Lai, X. Yin, and H. Liu, 'Impact of Inverter Interfaced Generators on Distance Protection', in *2019 4th International Conference on Intelligent Green Building and Smart Grid (IGBSG)*, Hubei, Yi-chang, China: IEEE, Sep. 2019, pp. 512–515. doi: 10.1109/IGBSG.2019.8886184.

[6] K. Ma, H. K. Høidalen, Z. Chen, and C. L. Bak, 'Improved Zone 1 Top-line Tilting Scheme for Polygonal Distance Protection in the Outgoing Line of Type-4 Wind Parks', *CSEE Journal of Power and Energy Systems*, vol. 9, no. 1, pp. 172–184, Jan. 2023, doi: 10.17775/CSEEJPES.2021.07870.

[7] L. Yuan, Z. Liu, J. Huang, F. Qiao, H. Yu, and T. Wen, 'COMPARATIVE STABILITY ASSESSMENT OF GRID-FOLLOWING AND GRID-FORMING VSCS IN WEAK GRIDS', in *The 10th Renewable Power Generation Conference (RPG 2021)*, , Online Conference: Institution of Engineering and Technology, 2021, pp. 496–502. doi: 10.1049/icp.2021.2288.

[8] M. Wang, K. Meng, L. Yu, L. Yuan, and Z. Liang, 'Comparative Fault Ride Through Assessment between Grid-following and Grid-forming Control for Weak Grids Integration', in *2022 IEEE Global Conference on Computing, Power and Communication Technologies (GlobConPT)*, New Delhi, India: IEEE, Sep. 2022, pp. 1–6. doi: 10.1109/GlobConPT57482.2022.9938233.

[9] Q. Liu, K. Jia, B. Yang, L. Zheng, and T. Bi, 'Fault Analysis of Inverter-Interfaced RESs Considering Decoupled Sequence Control', *IEEE Transactions on Industrial Electronics*, vol. 70, no. 5, pp. 4820–4830, May 2023, doi: 10.1109/TIE.2022.3181382.

[10] 'IEEE/IEC Measuring relays and protection equipment – Part 24: Common format for transient data exchange (COMTRADE) for power systems', *IEEE Std C37.111-2013 (IEC 60255-24 Edition 2.0 2013-04)*, pp. 1–73, Apr. 2013, doi: 10.1109/IEEESTD.2013.6512503.

[11] Aalborg University and K. Ma, 'Advanced Protection Schemes of Modern Transmission Grids with Large-Scale Power Electronics', Ph.d, Aalborg University, 2022. doi: 10.54337/aau478976808.